PHYS 4998 Final Report:

Exciton Polaritons: Strong Coupling between Monolayer Transition Metal Dichalcogenides and Dielectric Photonic Crystal Slab

Name: Qinxi Liu

Faculty Advisor: Bo Zhen

Mentors: Zhi Wang, Li He

Abstract

Strong coupling between light and matter opens up new possibilities for polaritonic devices such as spintronics, valleytronics, and non-linear light generators. Monolayer transition metal dichalcogenides (TMDs) are a promising candidate for such devices due to their direct bandgaps and high exciton binding energies. In this work, a mm-scale MoSe2 monolayer was obtained through gold exfoliation and passivated by 1-dodecanol encapsulation. It was coupled to a planarized photonic crystal slab to produce polaritonic bands. The weak signals of the angle-resolved reflectance spectra point out future directions to strengthen radiating modes for observing the strong coupling effect. The orthorhombic photonic crystal lattice contains Dirac points on resonance with the excitonic band, allowing future investigation in topological insulators.

Introduction

Strong coupling between excitons and photons generates polaritons, which are quasi-particles that lead to quantum many-body physics phenomena, enabling new photonic devices such as topological insulators [1], quantum simulators [2], and non-linear photon emitters [3]. One way to establish strong light-matter coupling is through semiconductor quantum wells in coupled microcavities [4], but the planar cavities are limited by inflexibility for band structure engineering, material compatibility, and bulkiness of the multilayer structures [5]. Recently, monolayer transition metal dichalcogenides (TMDs) become a promising candidate for polariton physics due to their direct bandgaps with enhanced quantum yield compared to their bulk counterpart, high exciton binding energies that support polaritons at room temperature [6], and the confined dipole orientation in two-dimensional structures that yield anisotropic excitonic emissions [7]. Strong coupling can be achieved by transferring monolayer transition metal dichalcogenides (TMDs) onto dielectric photonic crystal (PhC) slabs

[8], where excitons are coupled to the confined photons in the slab [5]. When the interaction rate between the exciton dipole and the photons occurs at a rate faster than the decay rates of the photon and the exciton, a polariton is formed with new eigenstates that are half-light, half-matter [6]. The strong coupling is then achieved. The PhC slab/TMD monolayer structure is highly flexible for mode engineering by varying the lattice patterns on a single chip.

Different from typically used μm-scale monolayer flakes, macroscopic monolayers have several benefits to couple with the PhC lattice. i) An mm-scale monolayer coupling with large PhCs (lateral size of 545 μm) ensures that the number of unit cells does not limit the mode quality factor. ii) A larger flake reduces the Fabry-Perot fringes caused by the mode reflection and interference at the monolayer boundary. iii) The monolayer flake covers an array of PhCs with different lattice constants allowing us to tune the wavelength of specific modes to match the exciton resonance. iv) Also, transferring one flake instead of many smaller flakes over the array significantly simplifies the fabrication, setting the stage for scalable applications of photonic devices.

Gold exfoliation is used to achieve macroscopic-size TMD monolayers. Conventionally, mechanical exfoliation using Scotch tape produces monolayers with high optical quality. For instance, a MoS_2 monolayer encapsulated by hexagonal boron nitride (hBN) reaches an exciton transition linewidth of 2 meV at T = 4 K [9]. However, in addition to low yield, the flakes are typically small with lateral dimensions <10 μm so they cannot fully cover the large PhCs. Larger flakes (~1 mm) can be obtained via ultra-flat gold tape [10], which has a larger van der Waals (vdW) attraction to 2D TMD materials than the TMD interlayer vdW force. This method allows a high success rate for monolayer exfoliation. However, the monolayers have impacted optical quality due to doping when in contact with the gold film, which contains charge carriers. Li et al. produced cm-scale TMD monolayers with uniformly high optical quality by encapsulating them in self-assembled 1-dodecanol molecular layers [11]. The $MoSe_2$ monolayer shows sharpened exciton linewidth from 26 ± 3 to 8.8 ± 1.3 meV over the 3-mm^2 flake after encapsulation and achieved a 7-fold improvement on photoluminescence quantum yield integrated over the exciton and trion resonances [11]. We are inspired to combine 1-dodecanol encapsulation with gold exfoliation to fabricate high-quality, macroscopic monolayers.

A square lattice of air cylindrical holes in Si_3N_4 slabs (refractive index n = 2.02) has doubly degenerate modes at the Γ point due to C_{4v} symmetry [12]. It is chosen as our lattice pattern because it emits modes at the Γ point, allowing the band structure to be measured at the far field with high resolution. A bare PhC square lattice has two bands with quadratic energy dispersion (ref [13], figure 3A). By shearing the square lattice into an orthorhombic lattice, spatial symmetries are broken and the two bands cross over near the Γ point to form two Dirac points, at which the dispersion becomes linear [12]. We are particularly interested in the photonic Dirac points because they can couple with the excitons in TMDs to produce topological phenomena, such as topological Chern insulators [1]. Hence, the orthorhombic lattice was fabricated as well to prepare for future investigation in topological photonics. To study the light-matter strong coupling, the exciton bands can be viewed as a highly degenerate flat band when incorporated into the photonic Brillouin zone because the excitonic unit cell size is ~10^3 smaller than that of the photons [1]. When the photonic bands are strongly coupled with the exciton dispersion-less band, two polariton bands emerge where the photonic and excitonic bands should have touched. Due to the energy splitting, the upper and lower polariton bands possess an anti-crossing nature. The energy separation where the photonic band meets the excitonic band, namely Rabi splitting, showcases the coupling strength, which scales with the excitonic dipole moment and electrical field. When a photonic Dirac point is approximately in resonance with the excitons, a Dirac cone generates a pair of polaritonic Dirac cones (ref [1], figure 2(d)). In a PhC slab with broken time-reversal symmetry, the degenerate excitonic band separates into distinct energy spectra, producing non-trivial topological effects. It is therefore possible to fabricate topological devices such as a Chern insulator [1]. This opens up a promising future direction for the TMD/PhC slab device.

In this work, we fabricated silicon nitride PhC slabs with square and orthorhombic lattices. Planarization using ALD SiO_2 improved the homogeneity of excitonic peaks and the improved z-axis symmetry separates polaritonic bands into distinguishable TE- and TM-like modes to observe strong coupling. An improved gold exfoliation and transfer method enhances the success rate of transferring macroscopic $MoSe_2$ monolayers onto patterned substrates in a controllable process. 1-dodecanol encapsulation of the $MoSe_2$ monolayer significantly improves its uniformity of optical quality. The band structure of the PhC slab/$MoSe_2$ monolayer device was obtained

through angle-resolved reflectance spectroscopy at T = 4 K, and the weak signals suggest future directions to enhance the capturing of strong coupling effects.

Procedure

The fabrication process of the PhC slab/MoSe2 monolayer device can be summarized in Figure 1. Mainly, e-beam lithography (EBL) patterned with a layer of 150 nm low-pressure chemical vapor deposition (LPCVD) silicon nitride on JGS2 fused silica substrate to produce the PhC lattice. The planarization involves forming a conformal film of SiO_2 over the structured substrate through ALD and polishing the oxide layer via chemical mechanical polishing (CMP). The gold-exfoliated monolayer was dry-transferred onto the PhC slab and the gold film was etched away to obtain the device. 1-dodecanol (1-DD) was coated before and after transfer to encapsulate the monolayer.

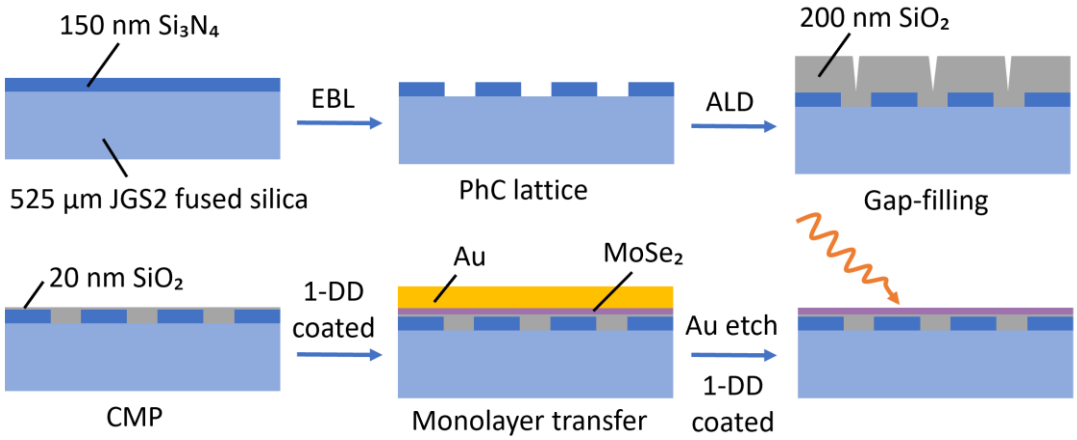

Figure 1. The fabrication process of the PhC slab/$MoSe_2$ monolayer device

E-beam lithography. LPCVD (Sandvik LPCVD, Sandvik Group) deposited a layer of 150-nm Si_3N_4 onto a 525-µm JGS2 fused silica substrate. The substrate was cut into 1 cm × 1 cm square pieces using a dicing saw. The wafers were cleaned with acetone in an ultrasonic cleaner for 10 minutes at 60°C, and then with isopropyl alcohol (IPA) for 5 minutes at 60°C. The wafers were rinsed with IPA in the ultrasonic cleaner for another 5 minutes and blown dry. Positive e-beam resist (ZEP520A-07, Zeon Corp.) was spin-coated onto the wafers at 2,000 rpm to form a layer thickness of 300 nm. The wafers were pre-baked at 180°C for 3 minutes to evaporate solvent. E-beam lithography system (EBPG5200+, Raith) patterned the wafers with square and orthorhombic lattices. Developer (o-Xylene, Sigma-Aldrich) cold-developed the e-beam resist at -8°C for 1 minute. The wafer was rinsed in the IPA for 1 minute. Reactive ion etching (Oxford 80

Plus RIE, Oxford Instruments) etched the resist for 5 minutes and the remover (KL 1000 Remover, KemLab) removed the resist for 10 minutes under 60°C with ultrasonic cleaning.. The wafers were cleaned in the piranha solution to remove resist residues.

Chemical Mechanical Polishing. ALD deposited a layer of 200-nm SiO_2 on the patterned wafers. The CMP tool (Logitech Orbis CMP, Logitech Ltd.) polished the oxide layer using a slurry (Semi Sperse SS12, Cabot) and a pad (Rodel IC1400, Rodel) down to 20 nm. Another alternate route produced the samples that were used to collect data below: in the PECVD tool (PlasmaLab 100 PECVD, Oxford Instruments), a liquid precursor tetraethyl orthosilicate (TEOS) was deposited onto the wafers and cured at 350°C to form a layer of 1-µm SiO_2. The oxide was polished down to 100 nm via CMP. Another layer of SiO_2 with a thickness of 10 nm was deposited using ALD. Figure 2 illustrates the different results using ALD and PECVD for planarization. ALD deposited conformal monolayers of atoms that effectively filled in the gaps in the structured substrate. After polishing, the SiO_2 surface achieved a high flatness. Comparatively, the PECVD-TEOS system could not completely conform to the structure substrate and formed voids during the thin-film growth. After polishing, the voids were exposed and produced an uneven surface. The patterned surface negatively impacted the monolayer optical quality. While conformal coatings are possible via the PECVD-TEOS system, one requires extensive parameter tuning. In addition, the poor quality of the PECVD oxide introduced inhomogeneous broadening to the monolayer that caused exciton peak shifting and broadening. Therefore, the first route was proposed as the preferred method.

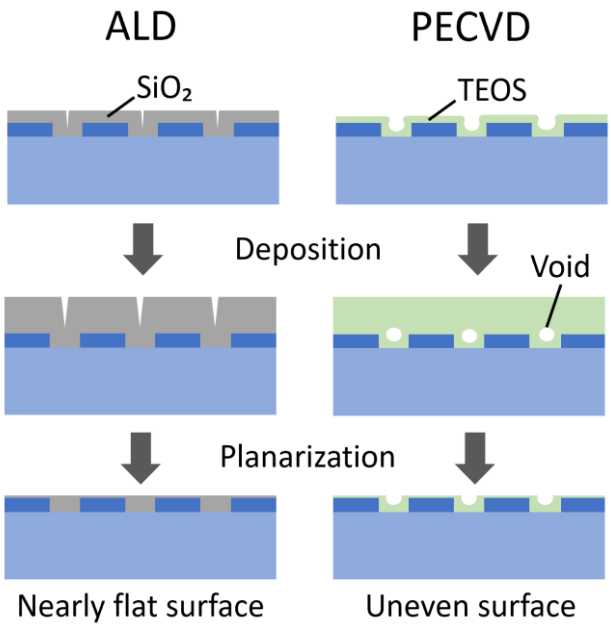

Figure 2. Comparison of planarization effect using atomic layer deposition (ALD) and plasma-enhanced chemical vapor-deposited (PECVD)

Gold Exfoliation and Transfer. A Si substrate with 90 nm SiO_2 was ultrasonically cleaned by acetone and IPA at 60°C. After being blown dry, the substrate was fixed on a holder using Kapton tape, and a 150-nm gold film was deposited using physical vapor deposition (PVD) (PRO Line PVD 75, Kurt J. Lesker Co.). A layer of polyvinylpyrrolidone (PVP) solution (10% wt in ethanol/acetonitrile wt 1/1, Sigma Aldrich) was spin-coated onto the gold tape at 1500 rpm for 2 min, with the acceleration of 500 rpm/s, and anneal at 150 °C for 2 min [15]. Another layer of polypropylene carbonate (PPC) solution was spin-coated on the gold tape to provide mechanical support. A piece of thermal release tape (TRT) with a square cutout (Figure 3(a)) picked up the gold tape. The gold film was suspended in the center of the TRT piece and adhered to its edges (Figure 3(b)). The gold film was pressed to a bulk $MoSe_2$ crystal and carefully peeled off to exfoliate a monolayer (Figure 3(c)). An undersized polydimethylsiloxane (PDMS) stamp went through the TRT cutout to come in contact with the gold film (Figure 3(d)). This method enhances the flexibility of the gold tape to thoroughly be in contact with the TMD bulk crystal and yield complete, large-scale monolayers. The PhC slab was coated with 1-dodecanol via the method in [15].

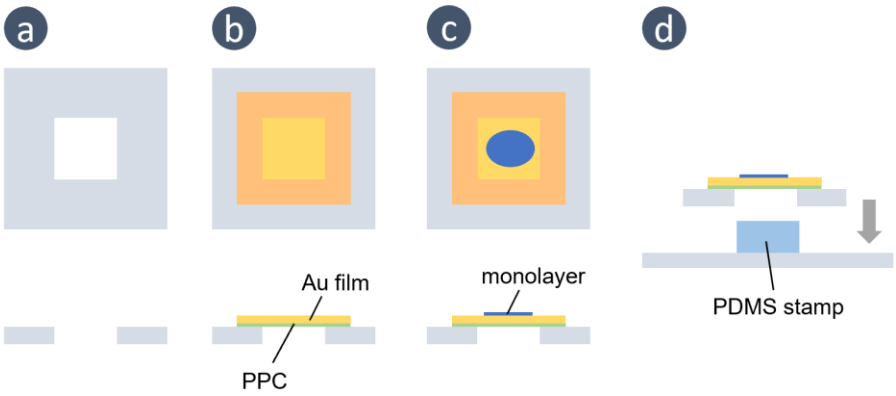

Figure 3. Process of gold-assisted exfoliating and transferring TMD monolayers

On the 2D transfer system (HQ2D MAN, HQ graphene), the PhC slab slowly came in contact with the gold tape/PDMS stack (Figure 4). A hot plate heated the stack to 180°C for 10 min. The transfer stage dropped fast to allow the detachment of the gold tape from the PDMS stamp. The gold tape/$MoSe_2$ monolayer was adhered to the PhC slab. The transfer stage is an improvement from hand-peeling TRT because the controllable transfer process ensures a high success rate and repeatability.

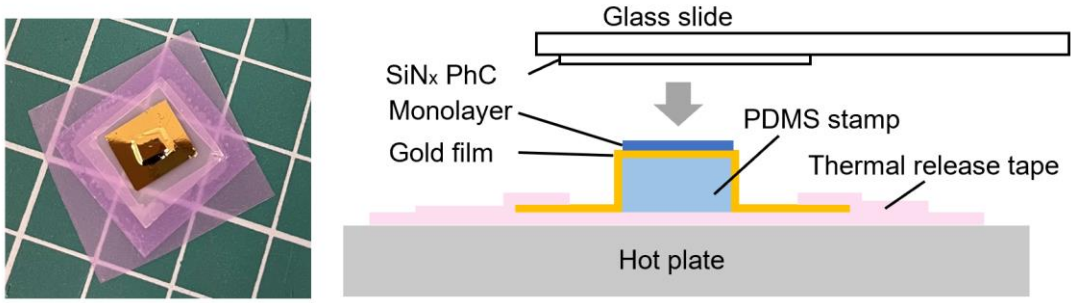

Figure 4. PDMS stack structure used to transfer $MoSe_2$ monolayers

Gold Etching. The PhC slab was immersed in acetone for 5 minutes, IPA for 5 minutes, and deionized (DI) water for 5 minutes. Gold etchant (Gold Etchant TFA, Transene Co. Inc.) was diluted by DI water with a ratio of 1:1. The PhC slab was etched for 5 minutes and rinsed with DI water. After being blown dry, another layer of 1-dodecanol was coated on the monolayer.

Results & Discussion

Optical Quality of Passivated $MoSe_2$ Monolayer. To verify the passivation effect of 1-dodecanol in producing high-quality TMD monolayers, a gold-exfoliated $MoSe_2$ monolayer was transferred to an unpatterned JGS2 substrate and encapsulated with 1-

dodecanol via the method specified in [11]. The low-temperature (T = 4K) photoluminescence (PL) (Figure 5(a)) and reflectance (R) spectroscopy (Figure 5(b)) measure the optical quality and uniformity of the monolayer by collecting data over 6 locations (pos1-6) spanning across 100 μm of the monolayer. A $MoSe_2$ monolayer was exfoliated by gold film and transferred to a JGS2 substrate without encapsulation. Its optical properties were measured as a comparison (pos A-B). The encapsulated monolayer shows a trion peak at 1.62 eV and an exciton peak at 1.65 eV (Figure 5(a)). Compared to the bare monolayer (pos A-B), the significantly reduced trion and exciton linewidths show the effectiveness of 1-dodecanol encapsulation in reducing the defect concentration. What's more, the reflectance spectra show that the exciton linewidth reduces from 17.8 ± 3.6 meV to 10.8 ± 1.3 meV (Figure 5(b)). On the other hand, the consistent peak profiles over pos 1-6 in PL and R spectra imply the enhanced uniformity of the monolayer optical quality. While pos A and B on the bare sample differ by ~ 20 meV in the trion peaks and no visible exciton peak is shown in pos B, the encapsulated sample (pos 1-6) shows consistent trion and exciton peaks with a variation within 4 meV (Figure 5(a)). The overlapping fano features at ~1.65 eV in the R spectra confirm that the monolayer has uniform qualities across a 0.01-mm^2 region.

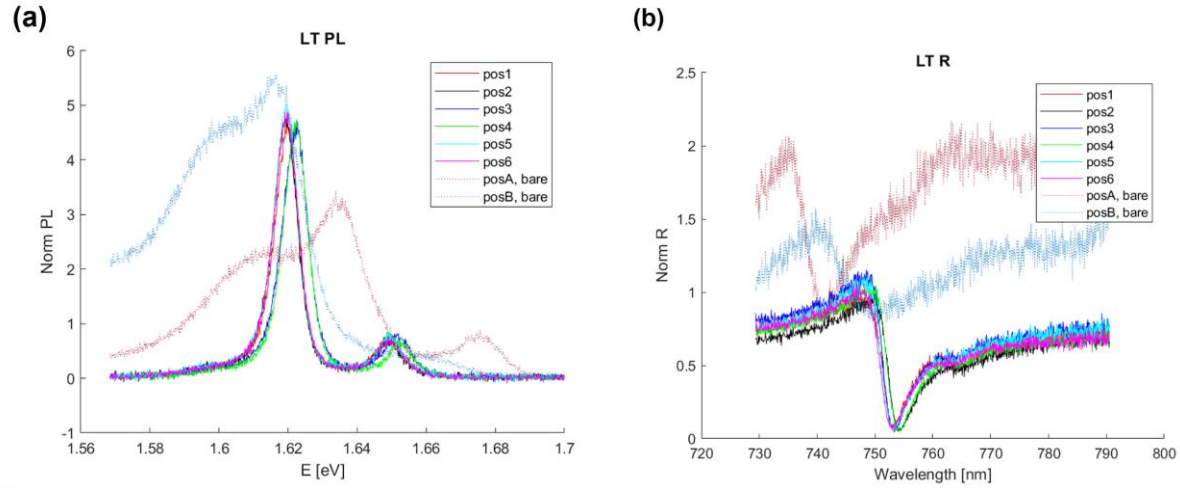

Figure 5. (a) Normalized PL and (b) reflectance spectra of a 1-dodecanol encapsulated $MoSe_2$ monolayer (pos 1-6) and a bare $MoSe_2$ monolayer (pos A-B)

Effect of Planarization on Monolayer Quality. After confirming the optical quality of 1-dodecanol-coated monolayers on the unpatterned JGS2 substrate, the next step is to measure the optical quality of the monolayer on top of the patterned PhC slab. Since the finite thickness of the slab loses mirror symmetry in z direction, the TE-like and TM-like modes become energetically similar and are hard to distinguish from the

measured band structure. To make the bands more resolved for observing the strong coupling effect, we need to maintain mirror symmetry by suspending the monolayer in the air [16] or filling the structured substrate with a layer of dielectric materials to resemble the refractive index of the JGS2 substrate. Additionally, the patterned regions experience severe inhomogeneous broadening, hindering the observation of polaritonic bands. For instance, in an hBN-encapsulated MoSe2 monolayer transferred to a Si/SiO_2 patterned substrate [16], the exciton peak locations varied significantly in the region without suspension (ref [16], Figure 1(c)). Comparatively, the suspended regions achieved improved spatial homogeneity as shown by an exciton energy variation less than the 1.5-meV linewidth [16]. Hence, we need to completely suspend the monolayer or planarize the substrate to improve the resolution and homogeneity of the polaritonic bands.

A complete suspension of mm-scale monolayer poses physical challenges to mechanically stabilize the flake and to keep it flat. The suspended monolayer is likely to bow out at the center, causing inhomogeneous broadening due to the non-flat surface. Hence, we used planarization by filling the patterned regions with a layer of SiO_2. Initially, a layer of 1-µm SiO_2 was grown by PECVD and polished down to ~100 nm. The PECVD planarization had two issues: i) PL spectra suggested that the PECVD-grown SiO_2 introduces additional doping to the $MoSe_2$ monolayer, resulting in a deviated exciton peak position. This is unsurprising because the optical quality of the monolayer depends strongly on the substrate material. Li et al.'s work shows an example of this effect, where the PL and R spectra of gold-exfoliated $MoSe_2$ monolayers vary drastically on fused silica and SiN_x substrates (ref [15], supplementary figure 6(a)-(b)). Hence, we switched to using ALD for planarization because its reaction process produces free-of-byproduct SiO_2 thin films with high optical quality [17]. ii) PECVD has poor surface coverage for the patterned substrate, forming voids between etched Si_3N_4 structures (see Figure 2). The voids contribute to uneven surfaces after polishing, which exacerbates inhomogeneous broadening after the monolayer is transferred on top. On the other hand, ALD can form conformal thin films on the structured surface (ref [18], Figure 1), so the polished surface reaches high flatness and helps reduce the monolayer excitonic linewidth.

To demonstrate the impact of the uneven surface formed by PECVD SiO_2 on monolayer

optical properties, a PhC slab was first planarized with ~100 nm PECVD SiO_2 and covered by a thin layer of polished ALD SiO_2 (~10 nm) to minimize the doping impact of PECVD TEOS oxide layer. Note that the thin layer of ALD oxide could only reduce the voids formed during PECVD instead of eliminating them. A gold-exfoliated $MoSe_2$ monolayer (Figure 6(a)) was transferred on top. Locations in patterned (Figure 6(b); p1-3, p9-10, p99) and unpatterned regions (Figure 6(b); p4-8) were sampled for PL and R spectroscopy.

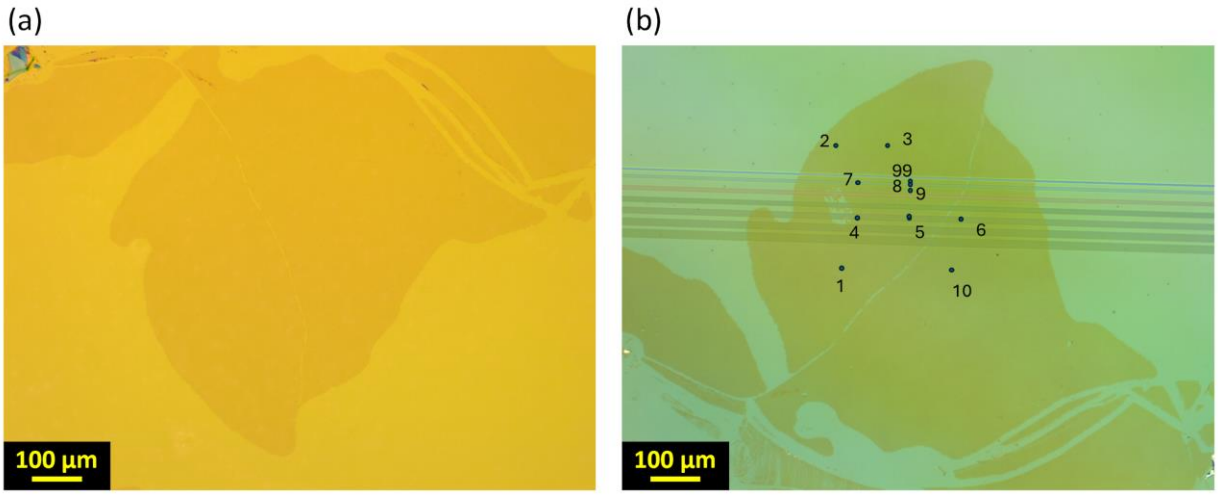

Figure 6. Optical microscopic images of the $MoSe_2$ monolayer (a) exfoliated on the gold film; (b) after transferring and etching. Both images were taken under 10x magnification. The labeled points in (b) were measured using PL and R spectroscopy to characterize the uniformity of the monolayer optical quality. The PhC slab in (b) was patterned with square lattices in the colored stripe regions.

Figure 7 shows the PL and R spectra for the sampled region on the PhC slab. Figure 7(a)-(b) probes the uniformity of optical qualities on the unpatterned PhC substrate. In the PL spectra, the trion peaks center at 1.621 ± 0.002 eV, and the exciton peaks center at 1.648 ± 0.001 eV. In the R spectra, the exciton fano feature occurs at 1.651 ± 0.001 eV. Despite that p2 has an exceptionally high yield, the small standard deviation of the peak locations (n = 6) suggests that the unpatterned regions have consistent optical qualities. Figure 7(c)-(d) compares the patterned regions (p5, p8) with the unpatterned (p9, p99). In the PL spectra, the quality factors of trion and exciton peaks decrease significantly in p5 and p8's profiles. p5 has an additional exciton peak at 1.64 eV, indicating severe inhomogeneous broadening in the patterned regions. The R spectra show that the exciton linewidth in the patterned region p8 broadens from 9.9 meV (p9) to 30.0 meV, which is comparable to the magnitude of Rabi splitting [1] [19] and hence will hinder the observation of strong coupling effect. Additionally, the p5 exciton peak

differs from that of p8 by 6 meV, further contributing to the inhomogeneous broadening of the patterned regions. To increase the flatness of structured substrates, the next step is to exclusively use ALD oxide for planarization.

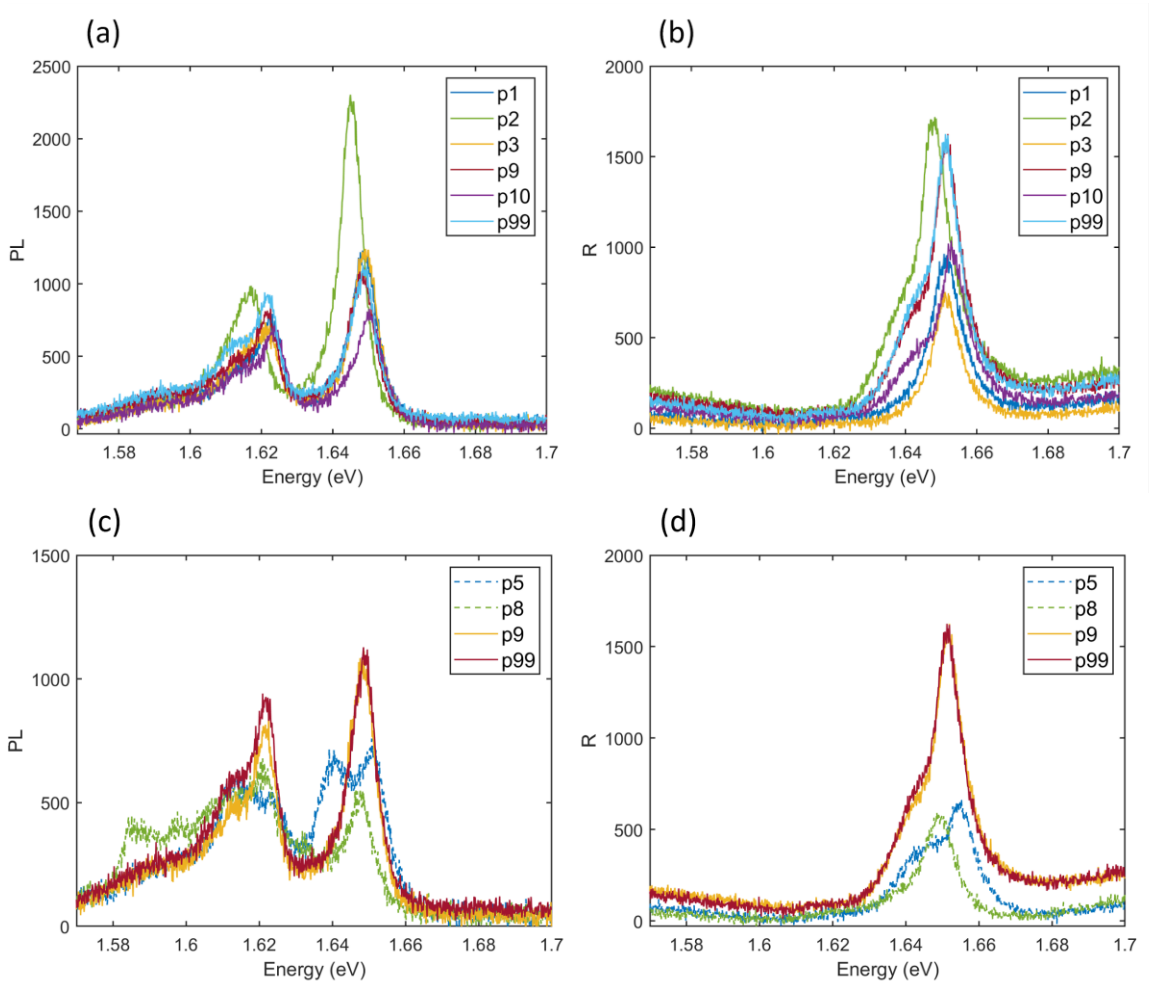

Figure 7. Photoluminescence (PL) and Reflectance (R) spectra of the $MoSe_2$ monolayer on (a)-(b) unpatterned PhC slab region, (c)-(d) comparison of patterned (dashed line) and unpatterned regions (solid line). p1-p99 are different measurement locations denoted in Figure 6(b).

Band Structure of PhC Slab/$MoSe_2$ Monolayer Device. A PhC slab/$MoSe_2$ monolayer was fabricated with an orthorhombic lattice with lattice constant a = 520 nm and a rhombus angle of 75°. The PhC slab was first planarized with PECVD SiO_2 and a layer of ALD SiO_2 was deposited to increase flatness and minimize doping. The monolayer was encapsulated by 1-dodecanol to ensure consistent optical quality. Figure 8 shows the microscopic image of the device after gold etching.

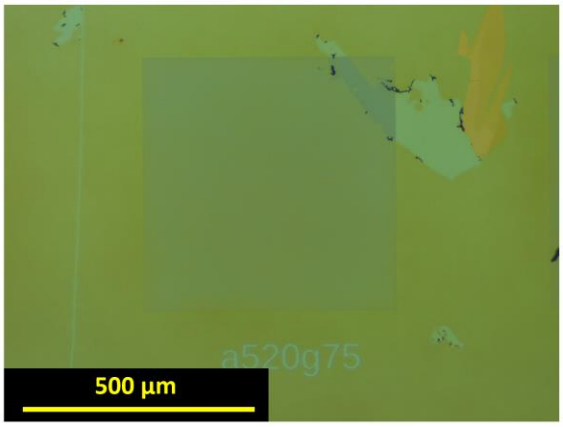

Figure 8. Optical microscopic image of the PhC slab/$MoSe_2$ monolayer device under 10x magnification. The PhC slab was patterned with an orthorhombic lattice (lattice constant a = 520 nm, rhombus angle = 75°). The planarization included a polished PECVD SiO2 layer with a thickness of 100 nm and a top layer of ALD SiO2 with a thickness of ~10 nm.

To measure the band structure of such a device, the angle-resolved reflectance spectrum of a patterned PhC slab was first measured at room temperature (Figure 9(a)) and the reflectance spectrum of the PhC slab/$MoSe_2$ monolayer device was probed at T = 4 K (Figure 9(b)). The room-temperature R spectra show the splitting of quadratic degeneracy to 1.67 eV and 1.63 eV at the Γ point and a Dirac point on resonance with the excitonic band (1.65 eV). The discontinuous bands are likely due to instrumental error. The low-temperature R (Figure 9(b)) only captures weak signals at energy 1.63 – 1.67 eV, so no strong coupling is observed yet. There are a few reasons as to why weak signals are observed: i) the intrinsic absorptivity (α) of the MoSe2 monolayer peaks at photon energy approximating the exciton's ($\alpha > 2 \times 10^{-5}\ cm^{-1}$ at photon energy ≈ 1.6 eV) (ref [20], Figure 2(e)) so the material absorbs part of the detectable radiating modes from the PhC slab. Another effect of the material absorption is an increased system loss and broadened exciton linewidth. Although both consequences are not desirable for observing strong coupling, photon absorption is necessary to excite an electron from the valence band to the conduction band to produce an exciton. Hence, we need to optimize other aspects to amplify the signals. ii) as indicated in Figure 7(c)-(d), the unevenly patterned surface exacerbates the inhomogeneous broadening of the excitons. As the in-plane exciton dipoles collide, the emitted photons are out-of-phase and modes destructively interfere, weakening the polaritonic signals. One future direction is to deposit the SiO_2 layer only through ALD to eliminate the rough surface formed during PECVD and the subsequent polishing process (Figure 2). A flatter

substrate will reduce the inhomogeneous broadening in the monolayer excitons and strengthen the signals. iii) The high quality factor of the PhC leads to smaller radiative loss, so fewer radiating modes can be observed. Planarization enhances the mirror symmetry in z-direction and homogeneity but confines more modes inside the PhC lattice. To obtain a sweet spot between the spatial homogeneity and the detectable amount of radiative loss, we will reduce the planarized SiO_2 layer thickness from the current ~110 nm (the total thickness of PECVD and ALD SiO_2 layers) to ~20 nm of ALD SiO_2 to moderately decrease the system symmetry.

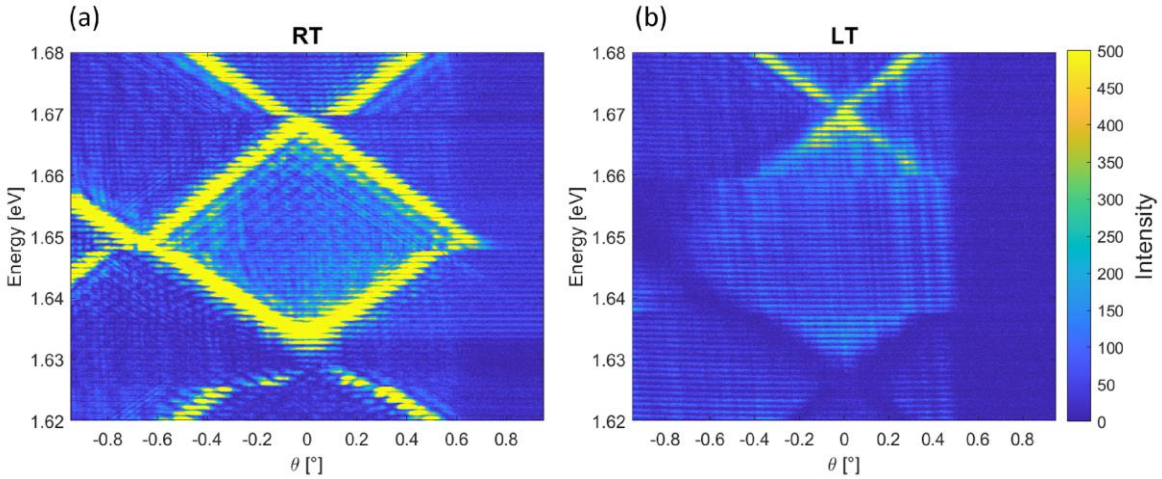

Figure 9. Angle-resolved reflectance spectra of (a) a bare PhC slab with an orthorhombic lattice at room temperature and (b) a PhC slab/MoSe2 monolayer device at T = 4 K.

Conclusion

A PhC slab/MoSe2 monolayer device was fabricated to generate polaritonic bands. The compact platform is highly flexible for engineering photonic modes by tuning the lattice patterns. Macroscopic $MoSe_2$ monolayers prepared by gold exfoliation ensure a large interaction area with the photonic modes for high coupling strength. Additionally, the mm-scale monolayers enable easy, consistent testing over an array of photonic crystals with varying parameters. Planarized PhC substrate via ALD improves the exciton homogeneity and the distinguishability of the polaritonic bands. 1-dodecanol encapsulation significantly improves the uniformity of monolayer optical quality. Our highly tunable platform allows investigating strong coupling effects to study the quantum many-body phenomena. Using an orthorhombic lattice with Dirac points on resonance with the excitonic band, the platform also enables the promising possibility of fabricating topological insulators.

References

[1] He, L., Wu, J., Jin, J., Mele, E. J., & Zhen, B. (2023). Polaritonic Chern insulators in monolayer semiconductors. Physical Review Letters, 130(4), 043801..

[2] Byrnes, T., Recher, P., & Yamamoto, Y. (2010). Mott transitions of exciton polaritons and indirect excitons in a periodic potential. Physical Review B, 81(20), 205312..

[3] Liew, T. C., & Savona, V. (2010). Single photons from coupled quantum modes. Physical review letters, 104(18), 183601..

[4] Klembt, S., Harder, T. H., Egorov, O. A., Winkler, K., Ge, R., Bandres, M. A., ... & Höfling, S. (2018). Exciton-polariton topological insulator. Nature, 562(7728), 552-556..

[5] Gogna, R., Zhang, L., Wang, Z., & Deng, H. (2019). Photonic crystals for controlling strong coupling in van der Waals materials. Optics Express, 27(16), 22700-22707..

[6] Liu, X., Galfsky, T., Sun, Z., Xia, F., Lin, E. C., Lee, Y. H., ... & Menon, V. M. (2015). Strong light–matter coupling in two-dimensional atomic crystals. Nature Photonics, 9(1), 30-34..

[7] Schuller, J. A., Karaveli, S., Schiros, T., He, K., Yang, S., Kymissis, I., ... & Zia, R. (2013). Orientation of luminescent excitons in layered nanomaterials. Nature nanotechnology, 8(4), 271-276..

[8] Liu, W., Ji, Z., Wang, Y., Modi, G., Hwang, M., Zheng, B., ... & Agarwal, R. (2020). Generation of helical topological exciton-polaritons. Science, 370(6516), 600-604..

[9] Cadiz, F., Courtade, E., Robert, C., Wang, G., Shen, Y., Cai, H., ... & Urbaszek, B. (2017). Excitonic linewidth approaching the homogeneous limit in MoS 2-based van der Waals heterostructures. Physical Review X, 7(2), 021026..

[10] Liu, F., Wu, W., Bai, Y., Chae, S. H., Li, Q., Wang, J., ... & Zhu, X. Y. (2020). Disassembling 2D van der Waals crystals into macroscopic monolayers and reassembling into artificial lattices. Science, 367(6480), 903-906..

[11] Li, Q., Alfrey, A., Hu, J., Lydick, N., Paik, E., Liu, B., ... & Deng, H. (2023). Macroscopic transition metal dichalcogenides monolayers with uniformly high optical quality. Nature communications, 14(1), 1837..

[12] Zhou, H. (2016). Tailoring light with photonic crystal slabs: From directional emission to topological half charges (Doctoral dissertation, Massachusetts Institute of Technology)..

[13] Zhen, B., Chua, S. L., Lee, J., Rodriguez, A. W., Liang, X., Johnson, S. G., ... & Shapira, O. (2013). Enabling enhanced emission and low-threshold lasing of organic molecules using special Fano resonances of macroscopic photonic crystals. Proceedings of.

[14] Johnson, R. W., Hultqvist, A., & Bent, S. F. (2014). A brief review of atomic layer deposition: from fundamentals to applications. Materials today, 17(5), 236-246..

[15] Li, Q., Alfrey, A., Hu, J., Lydick, N., Paik, E., Liu, B., ... & Deng, H. (2023). Macroscopic transition metal dichalcogenides monolayers with uniformly high optical quality. Nature Communications, 14(1), 1837..

[16] Zhou, Y., Scuri, G., Sung, J., Gelly, R. J., Wild, D. S., De Greve, K., ... & Park, H. (2020). Controlling excitons in an atomically thin membrane with a mirror. Physical review letters, 124(2), 027401..

[17] Hiller, D., Zierold, R., Bachmann, J., Alexe, M., Yang, Y., Gerlach, J. W., ... & Zacharias, M. (2010). Low temperature silicon dioxide by thermal atomic layer deposition: Investigation of material properties. Journal of Applied Physics, 107(6)..

[18] Murray, C. A., Elliott, S. D., Hausmann, D., Henri, J., & LaVoie, A. (2014). Effect of reaction mechanism on precursor exposure time in atomic layer deposition of silicon oxide and silicon nitride. ACS applied materials & interfaces, 6(13), 10534-10541..

[19] Li, M., Sinev, I., Benimetskiy, F., Ivanova, T., Khestanova, E., Kiriushechkina, S., ... & Khanikaev, A. B. (2021). Experimental observation of topological Z2 exciton-polaritons in transition metal dichalcogenide monolayers. Nature communications, 12(1),.

[20] Morozov, Y. V., & Kuno, M. (2015). Optical constants and dynamic conductivities of single layer MoS2, MoSe2, and WSe2. Applied Physics Letters, 107(8)..